Available online at www.eccomasproceedia.org
Eccomas Proceedia COMPDYN (2025) 1929-1941

ECCOMAS
Proceedia

COMPDYN 2025
10th ECCOMAS Thematic Conference on
Computational Methods in Structural Dynamics and Earthquake Engineering
M. Papadrakakis, M. Fragiadakis (eds.)
Rhodes Island, Greece, 15-18 June 2025

TIME-DEPENDENT STRUCTURAL RESPONSE OF REINFORCED CONCRETE BRIDGE PIERS CONSIDERING DEGRADATION PHENOMENA UNCERTAINTIES

P. A. Miglietta[1], G. Blasi[1], D. Perrone[1], F. Micelli[1], M.A. Aiello[1]

[1] Department of Engineering for Innovation, University of Salento
Via per Monteroni, Lecce (73100), Italy
e-mail: paoloandrea.miglietta@unisalento.it

Abstract

Recent studies have shown that building materials are strongly affected by degradation phenomena, which might result in facility collapses or loss of structural integrity and functionality. Regarding reinforced concrete structures, it is well-recognized that reinforcement corrosion is the main cause of deterioration and reduces both load-bearing capacity and ductility. The Italian infrastructure heritage consists mainly of reinforced concrete bridges approaching their lifespan, therefore predictive analyses are required to schedule retrofit interventions. Degradation processes are highly dependent on both weather parameters (e.g. relative humidity and average temperature) and structural detailing, such as the concrete cover thickness. Due to their inherent uncertainties, predictive analyses performed adopting a deterministic approach may lead to unrealistic, too conservative or unconservative evaluation of the structural safety level, respect to the possible different limit states. To address this issue, a detailed evaluation of the time-dependent structural response of a bridge pier was conducted in this work, accounting for the statistical distribution of stochastic parameters in the definition of the degradation scenarios. Performance-decay curves were defined for the first cracking moment, the yielding moment, and the ultimate moment, considering the effects of reinforcement corrosion rate, concrete cracking and creep.

Keywords: Reinforced concrete degradation, structural safety assessment, corrosion, probabilistic assessment, functionality curve, bridges

ISSN:2623-3347
Peer-review under responsibility of the organizing committee of COMPDYN 2025.
doi: 10.7712/120125.12541.24949

1 INTRODUCTION

In the middle of the last century, the increasing use of vehicles in Italy and worldwide led to the construction of a large number of motorways and infrastructures. Due to the complex topography of the Italian territory, several bridges and viaducts were built to cross valleys, lakes, rivers and other roads. Prestressed concrete (PC) bridges have been the most widely adopted structural solution because of their suitability for prefabrication and cost effectiveness [1]. In some cases, neither long-term physical effects of the building materials nor durability aspects were considered at the design stage. As a result, the Italian infrastructure heritage consists mainly of reinforced concrete (RC) bridges that are approaching their lifespan or require urgent maintenance works. However, existing bridges still play a key role in the road network and their decommissioning can result in significant social and economic impact.

The large number of bridge collapses that have occurred in recent decades has pointed out that structural deficiencies are often related to the ageing of construction materials. For example, the collapse of the Polcevera viaduct was triggered by the brittle failure of a corroded tendon [2].

It is well known that rebar corrosion and concrete cracking are among the most common and detrimental causes of deterioration in RC structures. Rebars corrosion may occur in two forms: uniform and localized. Typically, the former is carbonation-induced and leads to a uniform reduction in diameter both around the cross-section and along the rebar; the latter is chloride induced and results in localized pits and notches. In addition, the expansive reaction products induce tensile stresses in the surrounding concrete, leading to cracking and cover spalling.

The carbonation reaction occurs when CO_2 penetrates the concrete pores. The concrete mechanical properties are not directly affected by such reaction; however, the PH reduction below nine causes the destruction of the protective layer of the reinforcement. A large number of experimental measurements carried out on RC buildings exposed to open air revealed that the carbonation penetration over time is proportional to the square root of time in years and to the carbonation rate K, expressed in mm/year$^{0.5}$. This parameter is influenced by several factors, including relative humidity (RH), CO_2 content, w/c ratio, type of cement and curing time [3], [4].

The reduction in reinforcement diameter is governed by the corrosion rate (v_{corr}). Based on an extensive experimental campaign conducted in Spain, Andrade demonstrated that RH is the most influential weather parameter in such process. For RH values below 80% v_{corr} is negligible, whereas under near-saturation conditions, it can reach 100-200 μm/year [5]. Sung proposed a time-dependent model to suit estimate v_{corr} as a function of concrete cover depth, environmental temperature and RH [6].

Several attempts were made to model degradation phenomena using analytical formulations. Concrete cover cracking can be accounted for by reducing its compressive strength as a function of corrosion penetration, as proposed in the Vecchio and Collins model developed in 1986 [7] and modified by Coronelli and Gambarova in 2004 [8]. The reduction in the reinforcement cross-sectional area can be modelled by reducing the steel mechanical properties (e.g. yield strength, tensile strength and ultimate strain) as a function of the percentage mass loss [9].

Analytical models can be employed to assess structural performance over time or to simulate different degradation scenarios. Either deterministic or probabilistic approaches were adopted in the literature. Loreto et al. predicted the residual service life of an RC deck subjected to chloride attack [10]. Formisano et al. estimated the robustness index of an existing RC arch bridge by considering multiple damage scenarios induced by reinforcement corrosion and concrete cracking [11]. Biondini et al. analyzed the time-variant behaviour of a four-span continuous bridge considering the randomness involved in the deterioration process [12].

In this study, the time-dependent evolution of the structural performance of an RC bridge pier was investigated. The moment-curvature response of the bottom cross-section was considered as performance indicators to estimate the evolution of the flexural capacity of the pier over its service life. Reinforcement corrosion, concrete cracking and creep were taken into account as degradation phenomena. The inherent uncertainties associated with concrete cover thickness, concrete compressive strength, annual rainfall days, and RH were considered through their statistical distributions, defined according to literature. A Monte Carlo simulation was used to generate a wide range of degradation scenarios, enabling the assessment of the impact of the stochastic nature of deterioration processes on the structural performance over a 100-year period. Functionality curves were drawn to evaluate the evolution of the structural behaviour of the pier over time, considering the impact of uncertainties related to deterioration processes.

2 DEGRADATION MODELS

According to Tuutti's model, the corrosion process of RC structures can be divided into two phases: the initiation period and the propagation period. During the former, carbon dioxide penetrates the concrete cover, corrosion penetration is negligible, and mechanical performance is affected by only creep and shrinkage. After a specific period, known as the triggering time, the steel surface is reached by the CO_2, the protective layer around the reinforcement is destroyed and the corrosion reaction takes place. During the propagation period, the reduction in the reinforcement cross-sectional area, concrete cracking, and loss of bond strength should be considered when evaluating the long-term evolution of structural performance [13].

2.1 The creep effect

The creep effect leads to a progressive increase of strain in RC elements subjected to both high static and dynamic loads. The formulation proposed by [14] was adopted in this work, as shown in equation (1):

$$E_c(t)=\frac{E_{ci}}{\varphi(t,t_0)} \tag{1}$$

where E_{ci} is the concrete elastic modulus at 28 days and $\varphi(t,t_0)$ is the creep coefficient. Further details on φ evaluation may be found in [14].

2.2 Carbonation penetration

A comprehensive model to describe carbonation penetration over time is provided by [14], as shown in equation (2):

$$x(t)=\sqrt{2\cdot k_e\cdot k_c\cdot k_t\cdot R_{ACC,0}^{-1}\cdot C_s}\cdot W(t)\cdot\sqrt{t} \tag{2}$$

where k_e is the environmental function depending on RH, k_c is the execution transfer parameter depending on the curing time t_0, k_t is the regression parameter, $R_{ACC,0}^{-1}$ is the inverse effective carbonation resistance of concrete determined by accelerated carbonation tests, C_s is the CO_2 concentration in kg/m^3 and W(t) is the weather function, depending on the number of rainfall days per year with $h_{Nd} \geq 2.5$ mm. The evolution of carbonation depth over time is depicted in Figure 1a. The corrosion triggering time, T_i, can be estimated by substituting the concrete cover thickness in equation (2) and evaluating the time required for carbon dioxide to reach the rebar surface.

2.3 Reinforcement corrosion

Once the corrosion reaction is initiated, the cross-sectional area of the reinforcement decreases as a function of the corrosion rate v_{corr}. In this study, the model proposed by Sung for v_{corr} was employed [6]. Two formulations are proposed for the uncracked and cracked concrete respectively, as shown in equations (3)-(4):

$$v_{corr,u}=1.02\cdot e^{0.04\cdot T}\left(\frac{RH-45}{100}\right)^{\frac{2}{3}} c^{-1.36}\cdot t^{1.83} \tag{3}$$

$$v_{corr,c}=2.5\cdot v_{c,u} \tag{4}$$

where $v_{corr,u}$ and $v_{corr,c}$ are the corrosion rates in μm/year for the uncracked and cracked stages respectively, T is the average annual temperature in °C, RH is the environmental relative humidity, c is the concrete cover thickness in mm and t is the time in years.

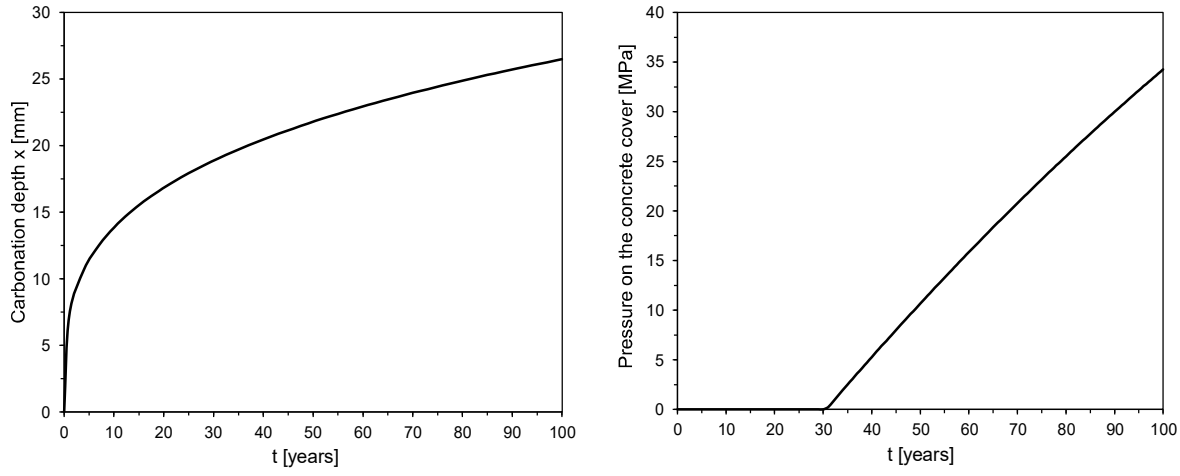

(a) (b)

Figure 1: (a) Evolution of carbonation penetration over time. (b) Evolution of the internal pressure on the concrete cover.

2.4 The effect of corrosion on steel mechanical properties

A number of experimental tests carried out on corroded rebar specimens pointed out that steel mechanical properties are deeply affected by corrosion. The relationships proposed by Imperatore [9] were adopted to account for rebars properties decay, as shown in equations (5)-(7):

$$f_{y,corr}=(1-0.0143453\cdot M_{loss}[\%])\cdot f_{y0} \tag{5}$$

$$f_{t,corr}=(1-0.0125301\cdot M_{loss}[\%])\cdot f_{t0} \tag{6}$$

$$\varepsilon_{u,corr}=e^{-0.0546993\cdot M_{loss}[\%]}\cdot\varepsilon_{u0} \tag{7}$$

where M_{loss} is the percentage mass loss, $f_{y,corr}$, $f_{t,corr}$ and $\varepsilon_{u,corr}$ are the corroded yield strength, the corroded tensile strength and the corroded ultimate strain respectively; while f_{y0}, f_{t0} and ε_u are the mechanical properties of the uncorroded steel. It is noteworthy that tensile strain, which

decays according to an exponential law, is the most affected parameter in case of corrosion and can induce a major reduction in local and global ductility.

2.5 Reduction in concrete-steel bond strength

Steel corrosion also leads to a reduction in concrete-steel bond strength. According to [15], the corroded concrete-steel bond strength can be evaluated as a function of the percentage mass loss M_{loss} [%], as shown in equation (8):

$$\tau_{bu,corr}=R\cdot\tau_{bu} \tag{8}$$

where τ_{bu} and $\tau_{bu,corr}$ are the uncorroded and corroded concrete-steel bond strength, respectively, and R represents a reduction parameter defined as shown in equation (9).

$$R=\begin{cases} 1 & \text{for } M_{loss}[\%] \le 6\% \\ 2.03e^{-0.118M_{loss}[\%]} & \text{for } M_{loss}[\%] > 6\% \end{cases} \tag{9}$$

2.6 Concrete cover cracking

The corrosion reaction generates expansion products that induce radial pressure P_{corr} on the surrounding concrete, resulting in concrete cracking. Several authors pointed out that the reinforcement is surrounded by a porous layer 10-20 μm thick [16], [17]. The expansion pressure takes place when such a layer is totally filled with rust. El Maaddawy [16] proposed a relationship between the percentage steel mass loss and P_{corr}. The concrete around the reinforcement is modelled as a cylinder of constant thickness submitted to internal pressure, as suggested by the elasticity theory [18]. Assuming that the corrosion products are formed uniformly around the rebar, P_{corr} can be evaluated using the equation (10):

$$P_{corr}=\frac{m_l E_{ef}\Phi}{90.1(1+\nu+\psi)(\Phi+2\delta_0)}-\frac{2\delta_0 E_{ef}}{(1+\nu+\psi)(\Phi+2\delta_0)} \tag{10}$$

where m_l is the percentage mass loss, E_{ef} is the concrete elastic modulus in MPa reduced due to the creep effect, ν is the concrete Poisson ratio, δ_0 is the thickness of the porous layer around the reinforcement in mm, Φ is the nominal rebar diameter in mm and ψ is a geometrical parameter evaluated through the equation (11). Negative values of P_{corr} mean that the porous layer is not yet totally filled by rust, therefore the internal pressure can be assumed equal to zero.

$$\psi=\frac{D^2}{2c(c+D)} \tag{11}$$

where $D=c+2\delta_0$. The evolution of radial pressure over time is shown in Figure 1b. Concrete cracking takes place when the circumferential stress achieves the concrete tensile strength f_{ct}. The radial pressure required to induce concrete cover cracking, P_{cr}, can be evaluated using equation (12):

$$P_{cr}=\frac{2cf_{ct}}{\Phi} \tag{12}$$

This phenomenon was considered through the model developed by Coronelli and Gambarova [8]. The concrete compressive strength of a circular region centered in the bar and with radius equal to concrete cover was decreased as indicated in equation (13):

$$f_c^* = \frac{f_c}{1 + K\frac{2\pi X n_{bars}}{b\varepsilon_{c2}}} \tag{13}$$

where f_c and f_c^* are the uncracked and cracked concrete compressive strength respectively, K is a coefficient equal to 0.1 for medium rebars, n_{bars} is the number of rebars in the compressive zone, X is the corrosion penetration in mm, ε_{c2} is the concrete strain at the peak and b is the width of the cross-section in mm.

3 DESCRIPTION OF THE PROBABILITY-BASED APPROACH

In this paper, a probability-based approach was employed to assess the long-term structural performance of an RC bridge pier. The evolution of the first cracking moment M_{cr}, the yielding moment M_y and the ultimate moment M_u over time were selected as performance indicators. The input parameters, including weather parameters, material properties and structural detailing were incorporated into the degradation models, to evaluate the impact of deterioration on the pier structural performance. The assessment follows the framework outlined in Figure 2 and is carried out over a 100-year period, with an annual time step. Functionality curves were drawn by plotting the temporal evolution of performance parameters.

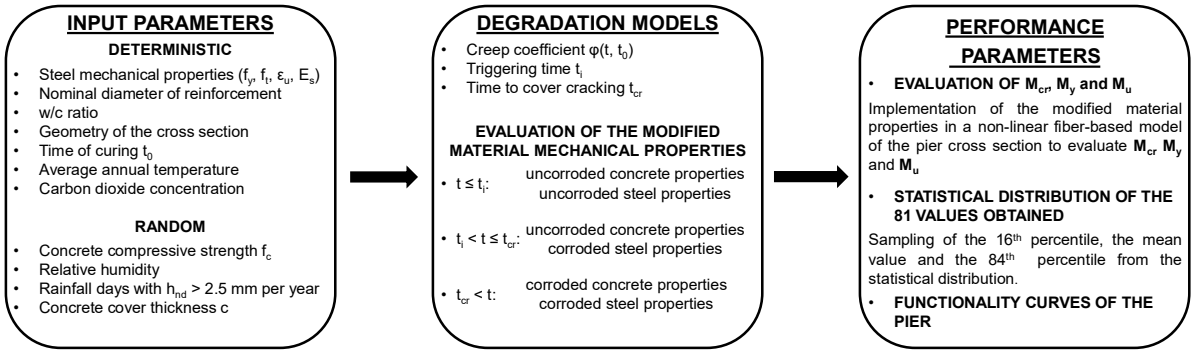

Figure 2: Framework for the evaluation of the performance parameters over time.

3.1 Description of the non-linear fiber-based approach and main assumptions

A fiber-based non-linear approach was employed to compute the performance indicators. Three distinct limit states were identified: first cracking, elastic limit and ultimate. The calculation of M_{cr}, M_y and M_u was conducted according to the following assumptions:

1. Sections that were plane before bending remain plane after bending, in accordance with the Euler-Bernoulli's assumption;
2. An elasto-plastic model with hardening was assumed for steel, whereas a linear piece-wise approximation of the Mander model was adopted for concrete in compression;
3. Rigid-plastic bond behavior at the concrete-rebar interface, peak bond strength computed according to equation (8).

Different failure mechanisms were considered in the computation of the resisting moment at each limit state

The first cracking limit state is defined by the attainment of the concrete ultimate tensile strain, ε_{ct}, at the tensile edge of the cross-section. The corresponding internal stress moment is denoted as M_{cr}.

The elastic limit state is reached when either the steel yielding strain, ε_{sy}, or the steel bond strain, ε_{bu}, is attained in the reinforcement. The resisting moment at this stage is denoted as M_y, regardless of the governing failure mechanism.

The ultimate limit state may be attained either when the concrete ultimate strain is reached at the compressive edge of the cross section or when ultimate steel strain is reached in the reinforcement. The resulting internal stresses moment corresponds to M_u.

To account for the effects of bar slip, the computation of M_{cr}, M_y and M_u of the pier cross-section was implemented in a spreadsheet using a macro-modeling fiber-based approach. The bond length at the bottom section was defined as the anchorage length within the foundation (850 mm).

3.2 Definition of functionality curves

First, all combinations of the random input parameters were generated. For each combination, both triggering time, t_i, and cracking time, t_{cr} were computed. At each time step and for each combination, the values of M_{cr}, M_y and M_u were evaluated for the bottom cross-section of the pier. A fiber-based analytical approach was adopted to compute neutral axis depth and internal forces distribution as function of the axial load and of the limit state considered. As long as $t \leq t_i$, corrosion process has not yet been triggered, thus the mechanical properties of the uncorroded material are employed in the analysis. For $t_i < t \leq t_{cr}$, rebars corrosion occurs, while the concrete is still in un-cracked stage. Therefore, only steel mechanical properties were modified as a function of percentage mass loss. Lastly, for $t > t_{cr}$, concrete cover cracking occurs and, consequently, both corroded steel and cracked concrete properties are considered in the analysis.

At each time interval, the statistical distributions of M_{cr}, M_y, and M_u were determined, and the relative 16^{th} (P16), 50^{th} (P50) and 84^{th} (P84) percentiles were sampled. Lastly, the functionality curves corresponding to each considered distribution bound were calculated by plotting the temporal evolution of the performance parameters.

4 ILLUSTRATIVE EXAMPLE

The process summarized by the framework shown in Figure 2 was applied to a RC bridge pier. The number of rainfall days per year, RH, concrete cover depth and concrete compressive strength were selected as random input parameters. The time-dependent evolution of the performance parameters described in section 3.1 was defined and functionality curves of the bottom pier cross-section were drawn. In addition, the influence of degradation phenomena and their stochastic nature on cross-section failure modes was investigated.

4.1 Description of the case study

The pier under investigation is part of RC bridge with nine simply supported spans. The upper deck is 10 m wide and consists in a 0.3 m thick RC slab supported by five prestressed concrete (PC) I-section beams having 1.2 m height, 0.5 m flange width, 0.15 m flange thickness and 0.12 m web thickness. The deck has span equal to 25 m. In Figure 3a-b both the pier cross-section and the shaft are depicted.

Ribbed steel rebars were adopted for concrete reinforcement, having yielding strength f_y=480 MPa, tensile strength f_t=570 MPa and ultimate strain ε_u=10%. The nominal diameter Φ of rebar is equal to 26 mm. The cylindrical characteristic compressive strength of concrete, f_c, is equal to 50 MPa, while the nominal concrete cover is 30 mm thick.

Two 25 m long spans are supported by the pier, transmitting an axial load of approximately 4000 kN, including both structural and non-structural dead loads.

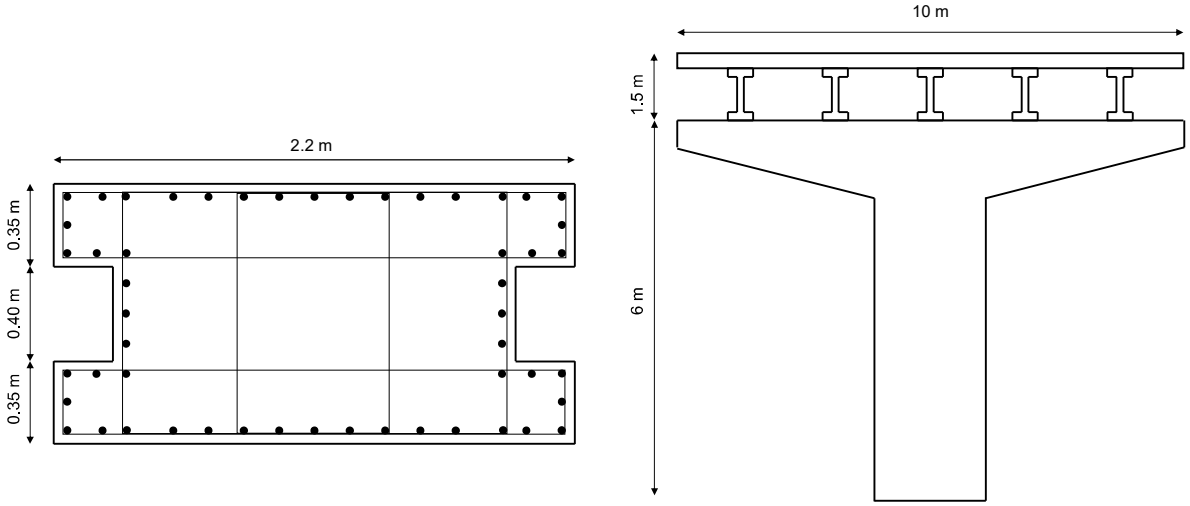

Figure 3: (a) Cross section of the pier, (b) Shaft of the pier and cross section of the upper deck.

4.2 Selection of the input parameters

In this study, both deterministic and random values of the input parameters were considered in the analytical models adopted to obtain the moment-curvature response of the pier. The values of the deterministic parameters were summarized in Table 1. Conversely, the influence of random parameters was considered through their statistical distribution.

The statistical distribution of both RH and rainfall days data was obtained from experimental measurements provided by hydrological annals [19]. The dispersion of such data is well-fitted by a normal distribution, as shown in Figure 4a-b. A normal distribution and a lognormal distribution were adopted for the concrete compressive strength and concrete cover depth, respectively (Figure 5a-b), as suggested by [14].

As the degradation processes are sensitive to the magnitude of the input parameters, a Monte Carlo simulation was carried out to generate a wide range of degradation scenarios. For each statistical distribution, the 16th percentile, the median value and the 84th percentile were sampled, as summarized in Table 2. A total number of 81 combinations of input parameters was generated for each year.

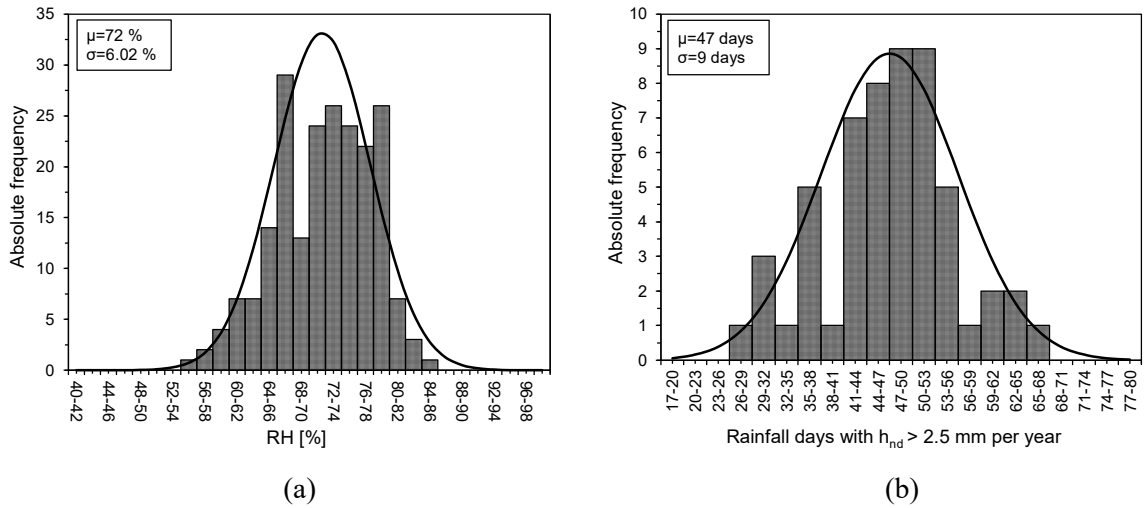

Figure 4: Statistical distributions of weather parameters: (a) RH, (b) rainfall days with h_{nd} > 2.5 mm per year.

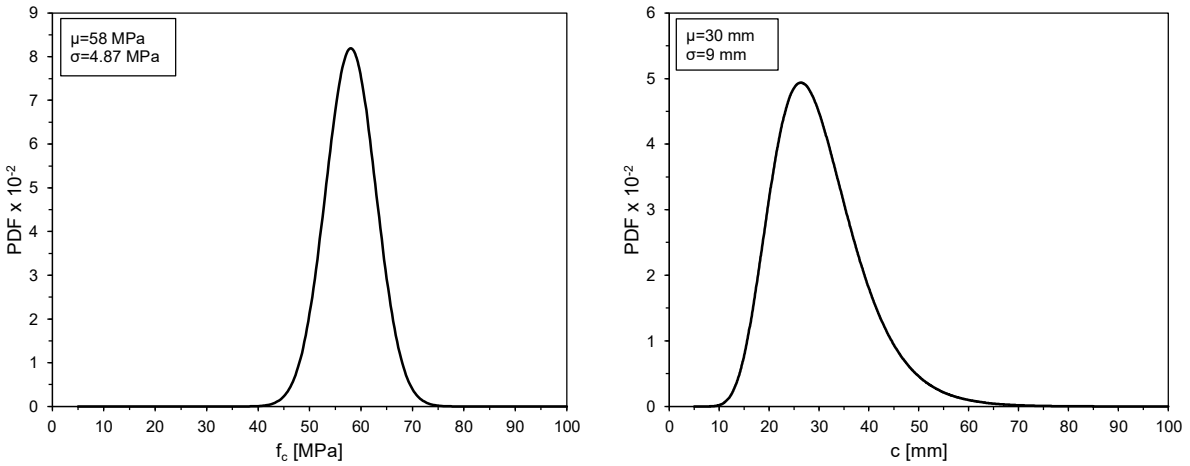

(a) (b)

Figure 5: (a) Statistical distribution of concrete compressive strength, (b) Statistical distribution of concrete cover thickness.

Parameter	Units	Value	Parameter	Units	Value
Steel yielding strength	MPa	480	CO_2 concentration	kg/m^3	0.0082
Steel ultimate strength	MPa	570	Concrete Poisson ratio	-	0.18
Steel ultimate strain	%	10	Thickness of porous layer	μm	10
Temperature	°C	20	Time of curing	days	28
Water/cement ratio	-	0.5	Reinforcement diameter	mm	26

Table 1: Deterministic input parameter values.

Parameter	Units	16^{th} percentile	50^{th} percentile	84^{th} percentile
Relative humidity	%	66	72	78
Rainfall days per year	-	38	47	57
Concrete cover thickness	mm	21	30	39
Concrete compressive strength	MPa	53	58	63

Table 2: Percentile sampled for random parameters.

4.3 Definition of functionality curves

The performance parameters of the bottom pier cross-section were calculated for each input combination and each year considered, in accordance with the assumptions outlined in section 3. For each year, P16, P50 and P84 were sampled from the statistical distributions of M_{cr}, M_y and M_u. The maximum and minimum values obtained over the reference period (100 years) were summarized in Table 3 and Table 4.

Parameter	Units	16^{th} percentile	50^{th} percentile	84^{th} percentile
First cracking moment M_{cr}	kNm	2741.02	2849.78	2957.95
Yielding moment M_y	kNm	7064.57	7108.32	7150.39
Ultimate moment M_u	kNm	9576.27	9680.76	9775.49

Table 3: Maximum values of M_{cr}, M_y and M_u referred to each percentile considered.

Parameter	Units	16^{th} percentile	50^{th} percentile	84^{th} percentile
First cracking moment M_{cr}	kNm	2037.75	2525.02	2862.34
Yielding moment M_y	kNm	2840.14	5461.32	6976.71
Ultimate moment M_u	kNm	2583.90	7246.31	9676.43

Table 4: Minimum values of M_{cr}, M_y and M_u referred to each percentile considered

The temporal evolution of the mean value of performance parameters along with the P16-P84 range is depicted in Figure 6a-c.

Since the first cracking moment depends on the tensile strength of concrete, at the construction stage (year 0), M_{cr} values mainly vary as function of the randomness of f_c. As long as $t<t_{cr}$, this variation remains nearly constant. Once corrosion-induced concrete cracking took place, M_{cr} values exhibit a significant reduction. Specifically, referring to the 16^{th} and the 50^{th} percentile curves in Figure 6a, concrete cracking due to corrosion occurs in the 60^{th} year, leading to a wider P16-P84 range of M_{cr} values.

The yielding moment is primarily influenced by the mechanical properties of steel, which were defined deterministically. Consequently, at the construction stage, M_y values are almost identical. However, as rebar corrosion progresses, a reduction in M_y becomes evident. Since the degradation of steel properties is strongly affected by percentage of mass loss, which is influenced by the randomness of both weather conditions and construction details, P16 curve exhibits a significant decrease over time (Figure 6b).

The ultimate moment is dependent on both concrete and steel properties, since the ultimate sectional capacity may be attained either due to concrete crushing or rebars tensile failure. At the construction stage, the curves show a slight difference associated with the randomness of the f_c value. The evolution of M_u exhibits the same trend observed in the elastic limit state (Figure 6c).

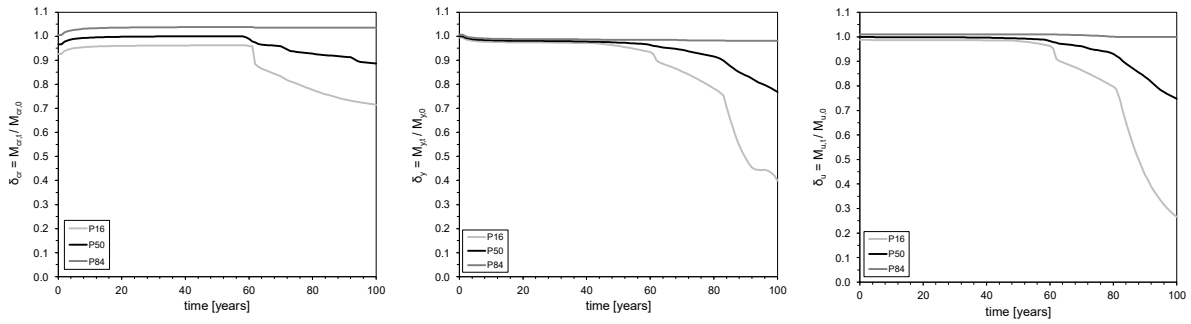

(a) (b) (c)

Figure 6: Evolution over time of performance parameters: (a) first cracking moment M_{cr}, (b) yielding moment M_y, (c) ultimate moment M_u.

The outcomes indicate that degradation phenomena have a major impact on the flexural capacity of the pier, and the variability of input parameters plays a crucial role in the temporal evolution of performance parameters. For instance, the triggering time calculated with the 84^{th} percentile of the concrete cover depth (39 mm) is higher than 100 years. Consequently, the corresponding performance parameters are not affected by degradation over time. For this reason, almost constant values were obtained referring to the 84^{th} percentile of the M_{cr}, M_y and M_u distributions.

Concluding, sectional performance over time may either remain nearly constant or exhibit substantial variations, as evidenced by the reduction percentage from time 0 to 100 years obtained for M_{cr}, M_y and M_u, as summarized in Table 5.

Parameter	16th percentile	50th percentile	84th percentile
ΔM_{cr} [%]	25.66	11.40	3.23
ΔM_y [%]	59.80	23.17	2.43
ΔM_u [%]	73.00	25.15	1.01

Table 5: Percentage change of M_{cr}, M_y and M_u referred to each percentile considered

4.4 Influence of stochastic input parameters on cross-section failure mode

The influence of the degradation phenomena and their uncertainties on the failure mode of the cross-section was examined. In Figure 7a-b the distributions of the failure modes of the cross-section are shown, referring to both the elastic limit state and ultimate limit state. With reference to the elastic limit state, reinforcement slippage may occur in in the last 20 years, due to the high level of corrosion. Hence, rebars contribution to resisting moment is not fully exploited as steel remains in the elastic range (Figure 7a).

Regarding the ultimate state, the assumption of the random variation of the concrete compressive strength value induces two different failure modes of the cross-section: concrete crushing and steel failure. Furthermore, from the 60th year onward, the progressive increase in corrosion levels results in higher concrete cracking, leading to a great reduction in its compressive strength. Consequently, the likelihood of the failure mode associated with concrete crushing increases with respect to that associated with steel failure.

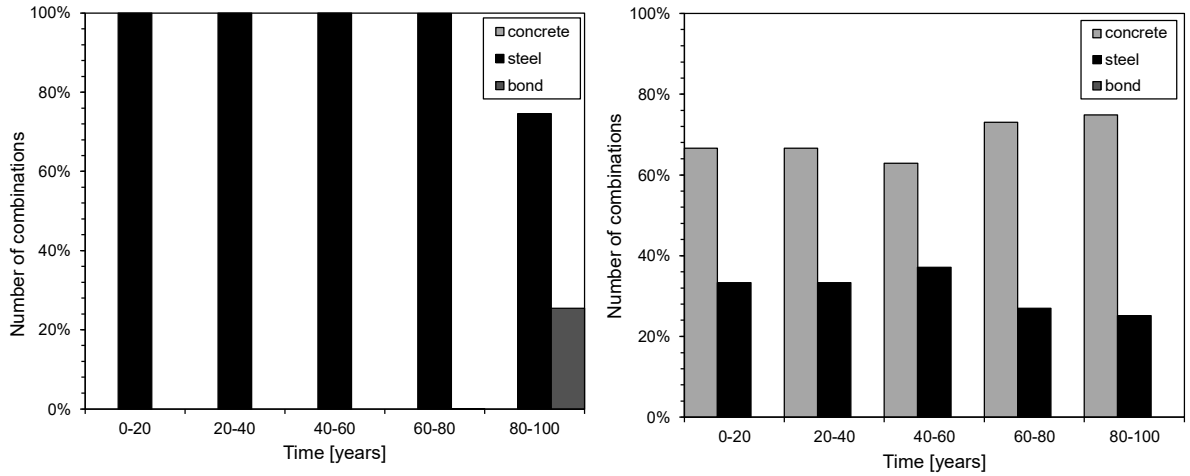

Figure 7: Distribution of cross-section failure mode: (a) elastic limit state; (b) ultimate limit state.

5 CONCLUSIONS

In this study, the effect of degradation phenomena on the structural performance of a RC bridge pier was investigated, accounting for the randomness of degradation driving factors such as weather parameters, material properties and construction details. The evolution over time of the first cracking moment, yielding moment and ultimate moment of the bottom cross-section of the pier was defined. The results highlighted that deterioration processes have a major impact on both functionality and load-bearing capacity of the element and may lead to a modification

of the failure mechanism ruling the flexural response. Furthermore, uncertainties in input parameters play a fundamental role in the temporal evolution of pier mechanical behaviour. In fact, flexural strength may either remain unchanged or exhibit a significant drop during the lifespan, depending on both weather conditions and construction detailing.

Predictive analyses of the case study pier behavior, conducted using a probabilistic approach, have highlighted several potential evolutions of the pier structural performance over time. Performance parameters can be calculated at discrete time steps through weather monitoring and structural diagnostics to aimed at assessing corrosion level, concrete cover depth or crack depth. Performance parameters obtained through in-situ inspections and measurements can be compared with the theoretical values defined according to the procedure outlined in this study. This comparison enables the assessment of the actual evolution of structural performance and the proper scheduling of maintenance and retrofitting activities.

6 ACKNOWLEDGMENTS

Funded by the European Union NexGeneration EU Research project Sustainable Mobility Center (Centro Nazionale per la Mobilità Sostenibile – CNMS) – Code CN00000023, CUP: F83C22000720001, SPOKE 7, approved for funding under Italian National plan for recovery and resilience (PNRR), MISSION 4 COMPONENT 2, INVESTMENT 1.4.

REFERENCES

[1] M. P. Petrangeli, *Progettazione e costruzione di ponti*, *4th ed*. Casa Editrice Ambrosiana, 1996.

[2] G. M. Calvi, M. Moratti, G. J. O'Reilly, N. Scattarreggia, R. Monteiro, D. Malomo, P. M. Calvi, R. Pinho, Once upon a Time in Italy: The Tale of the Morandi Bridge. *Structural Engineering International*, **29**, 98-217, 2019.

[3] A. Silva, R. Neves, J. de Brito, Statistical modelling of carbonation in reinforced concrete. *Cement & Concrete Composites*, **50**, 73-81, 2014.

[4] T. P. Hills, F. Gordon, N. H. Florin, P. S. Fennell, Statistical analysis of the carbonation rate of concrete. *Cement and Concrete Research*, **72**, 98-107, 2015.

[5] C. Alonso, C. Andrade, Life time of rebars in carbonated concrete. *Progress in the Understanding and Prevention of Corrosion*, 1994.

[6] Y. C. Sung, C. H. Huang, K. Y. Liu, C. H. Wang, C. K. Su, K. C. Chang, Life-cycle evaluation of deteriorated structural performance of neutralised reinforced concrete bridges. *Structure and Infrastructure Engineering*, **6** 741-751, 2010.

[7] F. J. Vecchio, M. P. Collins, The Modified Compression-Field Theory for Reinforced Concrete Elements Subjected to Shear. *ACI Journal*, 1986.

[8] D. Coronelli,P. Gambarova, Structural Assessment of Corroded Reinforced Concrete Beams: Modeling Guidelines. *Journal of structural engineering*, 2004.

[9] S. Imperatore, Z. Rinaldi, C. Drago, Degradation relationships for the mechanical properties of corroded steel rebars. *Construction and Building Materials*, **148**, 219-230, 2017.

[10] G. Loreto, M. Di Benedetti, A. De Luca, A. Nanni, Assessment of reinforced concrete structures in marine environment: A case study. *Corrosion Reviews*, **37**, 57-69, 2019.

[11] A. Formisano, M. Felitti, F. Oliveto, L. Mendicino, The robustness of reinforced con-crete tied arch bridges: A case study. *Structural Concrete*, **24**, 4504-4514, 2023.

[12] F. Biondini, E. Camnasio, A. Palermo, Lifetime seismic performance of concrete bridges exposed to corrosion. *Structure and Infrastructure Engineering*, **10**, 880-900, 2014.

[13] K. Tuutti, Corrosion of steel in concrete. 1982.

[14] FIB. Model Code for Concrete Structures 2010. 2013.

[15] L. Wang, *Strand Corrosion in Prestressed Concrete Structures*, Springer Ed, 2023.

[16] T. El Maaddawy, K. Soudki, A model for prediction of time from corrosion initiation to corrosion cracking. *Cement & Concrete Composites*, **29**, 168-175, 2007.

[17] B. Šavija, M. Luković, J. Pacheco, E. Schlangen, Cracking of the concrete cover due to reinforcement corrosion: A two-dimensional lattice model study. *Construction and Building Materials*, **44**, 626-638, 2013.

[18] S. Timoshenko, *Strength of materials*. Krieger Pub Co, 1976.

[19] https://www.regione.abruzzo.it/content/annali-idrologici.